

Published in final edited form as:

Nature. 2020 November 01; 587(7833): 309–312. doi:10.1038/s41586-020-2530-3.

Structural basis for RIFIN-mediated activation of LILRB1 in malaria

Thomas E. Harrison^a, Alexander M. Mørch^{a,b}, James H. Felce^b, Akihito Sakoguchi^{c,d}, Adam J. Reid^e, Hisashi Arase^{c,d}, Michael L. Dustin^b, Matthew K. Higgins^{a,*}

^a Department of Biochemistry, University of Oxford, South Parks Road, Oxford, OX1 3QU, UK

^b Kennedy Institute of Rheumatology, University of Oxford, Roosevelt Drive, Oxford, OX3 7FY, UK

^c Department of Immunochemistry, Research Institute for Microbial Diseases, Osaka University, Suita, Osaka 565-0871, Japan

^d Laboratory of Immunochemistry, WPI Immunology Frontier Research Center, Osaka University, Suita, Osaka 565-0871, Japan

^e Parasite Genomics, Wellcome Sanger Institute, Cambridge, United Kingdom

Abstract

The Plasmodium species that cause malaria are obligate intracellular parasites, and disease symptoms occur as they replicate within human blood. Despite risking immune detection, the parasite delivers proteins that bind host receptors to infected erythrocyte surfaces. In the causative agent of the most deadly human malaria, Plasmodium falciparum, RIFINs form the largest erythrocyte surface protein family¹. Some RIFINs can bind inhibitory immune receptors, acting as targets for unusual antibodies containing a LAIR1 ectodomain²⁻⁴, or as ligands for LILRB1⁵. RIFINs stimulate LILRB1 activation and signalling⁵, thereby potentially dampening human immune responses. To understand this process, we determined a structure of a RIFIN bound to LILRB1. We show that the RIFIN mimics the natural activating ligand of LILRB1, MHC class I, in its LILRB1-binding mode. A single RIFIN mutation disrupts the complex, blocks LILRB1 binding by all tested RIFINs and abolishes signalling in a reporter assay. In a supported lipid bilayer system, which mimics NK cell activation by antibody-dependent cell-mediated cytotoxicity, both RIFIN and MHC are recruited to the NK cell immunological synapse and reduce cell activation, as measured by perforin mobilisation. Therefore, LILRB1-binding RIFINs mimic the binding mode of the natural ligand of LILRB1 and suppress NK cell function.

Users may view, print, copy, and download text and data-mine the content in such documents, for the purposes of academic research, subject always to the full Conditions of use:http://www.nature.com/authors/editorial_policies/license.html#terms

* Correspondence should be addressed to: matthew.higgins@bioch.ox.ac.uk.

Author contributions

T.E.H. produced proteins, and conducted biophysical analysis. T.E.H. and M.K.H. determined the crystal structure. A.M.M., J.E.F. and M.L.D. designed, conducted and analysed supported lipid bilayer imaging experiments. A.S. and H.A. designed, conducted and analysed reporter assay studies and flow cytometry studies of RIFIN mutants. T.E.H. and A.J.R. performed bioinformatics experiments. T.E.H. and M.K.H. devised the study and drafted the manuscript. All authors discussed the results, contributed figures and text and commented on the manuscript.

Competing interests: The authors confirm that there are no competing interests.

Author information statement: All correspondence relating to this manuscript should be addressed to matthew.higgins@bioch.ox.ac.uk

To determine the molecular basis for RIFIN-mediated LILRB1 activation, we assessed expression of different fragments of a LILRB1-binding RIFIN ectodomain from the 3D7 strain of *Plasmodium falciparum* (PF3D7_1254800)⁵. RIFIN ectodomains contain N-terminal semiconserved domains and C-terminal variable domains, followed by transmembrane helices^{6,7}. While the full-length ectodomain did not express in a folded form, we produced the variable region (residues 165-274), previously shown to bind LILRB1, and the constant region (residues 39-139) (Extended Data Figure 1)⁵. While the constant region showed no binding, the variable region bound LILRB1 with $K_D = 570 \pm 130$ nM. This is comparable to the binding affinities of LILRB1 for MHC class I molecules, which range from 2 to 7 μ M⁸.

The monomeric variable domain was complexed with the complete extracellular domain of LILRB1, containing four immunoglobulin-like domains (Extended Data Figure 1b), allowing formation of crystals which diffracted to 3.0 Å. The structure was determined by molecular replacement, using existing structures of LILRB1 domains^{9,10} as search models (Figure 1, Extended Data Table 1). The LILRB1-binding region of the RIFIN adopts a primarily α -helical structure, consisting of three main helices. These are connected by extensive loops, which contain short helical segments (Figure 1a). Other proteins of the infected erythrocyte, such as DBL and CIDR domains of PfEMP1, are also built from small helical scaffolds¹¹, but do not share the topology of the RIFIN variable domain. In the RIFIN, cysteine C223 is unpaired and exposed to solvent, possibly forming an additional disulphide bond with a cysteine in the constant region when in the full ectodomain. For all subsequent experiments, we therefore designed a shorter and more stable RIFIN, removing disordered regions and mutating this free cysteine to serine (C223S). Surface plasmon resonance studies showed C223S to bind LILRB1 with $K_D = 700 \pm 5$ nM (Extended Data Figure 2). The remaining two cysteines form a disulphide bond that stabilises the complex loop that links the second and third main helices and forms most of the LILRB1 contact surface (Figure 1b,c).

The RIFIN binding site is contained within the two N-terminal, membrane distal immunoglobulin-like domains of LILRB1, as confirmed by surface plasmon resonance measurements (Extended Data Figure 2). Binding is mediated by loops at the interface between these two LILRB1 domains. The four LILRB1 domains form a linear 'zig-zag' arrangement. Previous structures of LILRB1 domains 1 and 2, alone¹² and in complex with MHC class I molecules¹⁰ have shown a $\sim 15^\circ$ widening of the angle between domains 1 and 2 on MHC binding. The structure in the presence of RIFIN is closer in angle to the unbound form (a $\sim 5^\circ$ widening), suggesting that the RIFIN does not cause a large conformational change in LILRB1.

The RIFIN contains an elongated LILRB1 contact site, formed from residues in the loop that lies between helices 2 and 3 (contributing $\sim 50\%$ of the 750 \AA^2 binding surface), the small loop that lies between helices 1 and 2 ($\sim 20\%$ of the contact area) and three side chains that lie along one side of helix 3 ($\sim 30\%$ of the contact area) (Figure 1c, Extended Data Table 2). The interaction has a small hydrophobic component, mediated by residues L230 and M235

of the RIFIN, which pack against a hydrophobic surface of LILRB1. This is complemented by hydrogen bonds involving RIFIN side and main chain groups.

To confirm that this binding interface is that used in a cellular context, we designed a G234R mutant of the RIFIN variable region, which introduces a bulky side chain predicted to sterically block LILRB1 binding (Figure 2a). While circular dichroism analysis suggested no significant change in RIFIN structure or stability (Extended Data Figure 1), surface plasmon resonance analysis showed that G234R decreased the affinity for LILRB1 to close to undetectable (Figure 2b, Extended Data Figure 2). We next assessed the effect of this mutation in a cellular assay (Figure 2c). A previous study used a nuclear factor of activated T cells (NFAT)-GFP reporter system in which GFP expression is induced upon LILRB1 binding to show that RIFINs can stimulate LILRB1-mediated signalling⁵. When we incubated these LILRB1-reporter cells with the RIFIN variable region, GFP expression was observed, while the G234R mutant induced no LILRB1 signalling in this system (Figure 2c, Extended Data Figure 3). This indicates that the interface observed in the crystal structure is that involved in induction of LILRB1-mediated signalling

We next assessed whether structural insight could allow us to identify a motif conserved in LILRB1-binding RIFINs. We compared structure-guided sequence alignments for the variable domains of all 185 RIFINs from the 3D7 strain of *P. falciparum* with those for the ten known LILRB1-binding RIFINs⁵. A sequence LOGO for the full RIFIN set showed little sequence conservation, other than of the two cysteines which form the disulphide bond (Extended Data Figure 4). This disulphide anchors the loop of the variable region which makes most of the interactions with LILRB1, and its conservation across the RIFIN family suggests that it may be important for ligand binding by other RIFINs. The LILRB1-binding RIFINs are similarly lacking in conservation, with even the residues which form direct interactions with LILRB1 showing significant variation (Extended Data Figure 4, Figure 2de).

We next assessed whether other LILRB1-binding RIFINs share a binding mode with 1254800 by making mutations equivalent to G234R and assessing their effect on LILRB1 binding. We first produced the variable domain of PF3D7_0100400 and showed binding to LILRB1 by surface plasmon resonance with $K_D = 4.4 \pm 3.2 \mu\text{M}$ (Figure 2f). This RIFIN has a leucine in the equivalent position to G234 and this L264R mutation disrupted binding (Figure 2f), without affecting the structure as assessed by circular dichroism (Extended Data Figure 5ab). We also used flow cytometry to quantify binding of LILRB1-Fc to erythrocytes infected with transgenic parasites expressing specific RIFINs⁵. G234R abolished LILRB1-binding by 1254800 in this assay. The equivalent mutations in two other RIFINs, G240R of PF3D7_1100400 and S244R of PF3D7_0100200, also prevented LILRB1 binding (Figure 2g, Extended Data Figure 5c). Therefore, while there is no defined sequence motif which characterises the LILRB1-binding RIFINs, mutagenesis shows that they use a shared binding loop and bind through a similar structural mechanism. This is reminiscent of the PfEMP1 proteins from *Plasmodium falciparum*-infected erythrocytes, in which extensive sequence variation is possible, even within a group of surface proteins that bind to the same endothelial receptors, allowing them to maintain function while diversifying to allow antigenic variation and avoidance of immune detection¹³⁻¹⁵.

We next compared the binding mode of the RIFIN with that of the physiological ligands of LILRB1; MHC class I molecules, such as HLA-A2¹⁶. We compared a structure of HLA-A2 bound to LILRB1 domains 1 and 2¹⁰ with that of the RIFIN-LILRB1 complex, by aligning the two complexes using the D1-D2 hinge (residues 96-103) (Figure 3a-c). This revealed that, while RIFIN and MHC class I molecules have very different structures, they share a binding site on LILRB1. The majority of the interactions between HLA-A2 and LILRB1 are formed between the β_2 -microglobulin (β_2 M) chain of the MHC and the LILRB1 D1-D2 interface (Figure 3b)¹⁰. This shares a number of features with the RIFIN. In particular, hydrogen bonds formed between the backbone of residues in the F-G strand loop of β_2 M are with the same LILRB1 residues as the interactions formed by RIFIN residues G234 and N236. Indeed, structure of the RIFIN loop containing these residues shares a similar conformation to that of the F-G loop of β_2 M (Figure 3c). The surface areas of the LILRB1 binding sites are also similar, with 750Å² for the RIFIN and 833Å² for a typical MHC class I. In addition, the length of the longest axis of the RIFIN:LILRB1 complex is very similar to that of the RIFIN:MHC class I complex. As the dimensions of immune complexes are important for their distribution within the immunological synapse¹⁷, this aspect of molecular mimicry may also contribute to the ability of the RIFINs to modulate LILRB1-mediated signalling. This suggests that RIFINs mimic the binding mode of HLA-A2, despite their lack of sequence or structural identity.

The similar binding mode of the RIFIN and MHC class I to LILRB1 raised the question of whether RIFINs stimulate LILRB1-mediated signalling through the same mechanism as MHC class I. Many immune receptors function through regulated recruitment to immunological synapses formed between immune cells and their targets^{17,18}. We therefore asked whether the RIFIN localises to the immunological synapse formed between immune cells and a supported lipid bilayer (SLB) and whether it modulates immune cell activation (Figure 3d-g). To determine which immune cells to study, we measured LILRB1 expression in peripheral white blood cells by antibody staining and flow cytometry, and found that, while LILRB1 is widely distributed, it is most prevalent in CD4⁺ T cells and NK cells (Extended Data Figures 6). Of these, NK cells are most relevant in the context of malaria blood stage infection as they have recently been shown to interact with infected erythrocytes through antibody- dependent cell-mediated cytotoxicity (ADCC)^{19,20}.

To mimic the contacts formed during ADCC we triggered formation of NK cell synapses by coupling human IgG1 and ICAM-1 to SLBs. The Fc region of the antibody engages CD16, while ICAM-1 forms an adhesive interaction with LFA-1. We then added equal densities of fluorescently labelled MHC class I, RIFIN or G234R to the SLBs before incubating with primary NK cells. Cells from three independent donors were incubated with the SLBs and were fixed and stained for LILRB1 and perforin, as a marker of NK cell activation, before analysis using total internal reflection fluorescence microscopy to examine the contact area and its associated fluorescent signals (Figure 3d, Extended Data Figures 7 and 8). We first noted that both MHC class I and RIFIN became enriched in the contact area while no enrichment of G234R was observed (Figure 3e). Furthermore, both MHC class I and the RIFIN showed positive, although incomplete, co-localisation with LILRB1 (Figure 3f). Therefore, the RIFIN localises to the synapse and this can be prevented by disrupting LILRB1 binding. Finally, we observed that perforin was recruited to the synapse in control

NK cells, indicating activation (Figure 3g). This was abolished in the presence of MHC class I, or RIFIN, but not G234R. Therefore, recruitment of a LILRB1-binding RIFIN to the immunological synapse, through the characterised LILRB1 binding site, caused loss of a marker of NK cell activation.

In summary, our structural analysis reveals that RIFINs can mimic the natural ligand of LILRB1, using a sequence-diverse surface to contact the same region of LILRB1 contacted by MHC class I. Specific disruption of this interaction by a single point mutation abolishes binding of four different LILRB1-binding RIFINs to LILRB1 and abolishes the effect of the RIFIN on LILRB1-mediated signalling. Both RIFIN and MHC class I show similar spatial distribution and similar levels of co-localisation with LILRB1 in an immunological synapse model of ADCC, as well as having similar negative effects on a marker of NK cell activation. This reveals that the parasite uses molecular mimicry to interact with an inhibitory immune receptor and to modulate receptor signalling. This potentially dampens the immune response to malaria, facilitating parasite survival, prolonging the infection and increasing transmission.

Methods

Protein expression and purification

Coding sequences for LILRB1 D1D4 and D3D4 (Gly1-Leu394 and Val199-Leu394 respectively, numbered as for the mature polypeptide), and the RIFIN constant region (PF3D7_1254800 39-139), were cloned into the pHLsec vector, giving a C-terminal His6 tag. These were transfected into HEK293F cells (ThermoFisher Scientific, UK) using polyethylenimine, and after 5 days were harvested by centrifugation at 5000xg. The cells were not authenticated or mycoplasma screened as cells were used for protein production rather than forming part of analysis. The supernatant was buffer exchanged into 20 mM HEPES pH 7.5, 150 mM NaCl, 20 mM imidazole by tangential flow filtration, and the protein purified by immobilised metal affinity chromatography using Ni²⁺-NTA resin with elution into 20 mM HEPES pH 7.5, 150 mM NaCl, 300 mM imidazole, followed by size exclusion chromatography using a Superdex 75 10/300 column (GE Healthcare).

LILRB1 D1D2 (Gly1-Gly198) and the RIFIN variable region (PF3D7_1254800 165-274) were cloned into a pET15b vector with an N-terminal His6 tag. The C223S and C223S G234R mutations of the RIFIN were incorporated by site directed mutagenesis and these constructs were recloned with domain boundaries 165-261. Constructs were transformed into BL21 (DE3) Competent *E. coli* (New England Biolabs), with expression induced at an optical density at 600 nm of 0.6 by adding isopropyl (β -D-1-thiogalactopyranoside to a final concentration of 1 mM. Proteins were purified from inclusion bodies as previously described⁵. Briefly, inclusion bodies were solubilised in 6 M guanidine hydrochloride, 20 mM Tris pH 8, 300 mM NaCl, 20 mM imidazole, and the denatured recombinant protein was purified by immobilised metal affinity chromatography using Ni²⁺-NTA resin, with elution into buffer containing 6 M guanidine hydrochloride, 20 mM Tris pH 8, 300 mM NaCl, 500 mM imidazole. Refolding was performed by flash dilution into 1 M L-arginine, 100 mM Tris pH 8.5, 2 mM ethylenediaminetetraacetic acid, 0.1 mM phenylmethylsulfonyl fluoride, 3 mM reduced glutathione and 0.3 mM oxidized glutathione, and the protein was

purified by size exclusion chromatography using a Superdex 75 10/300 (GE Healthcare) column in buffer 20 mM HEPES pH 7.5, 150 mM NaCl. The PF3D7_0100400 variable region (165-329) was expressed and purified using the same method, with the addition of 15% glycerol to the flash dilution buffer. Protein gels are all shown in Supplementary Figure 1.

Crystallisation, data collection, and structure determination

LILRB1 D1D4 and the RIFIN variable region were combined to a 1:1 molar ratio and incubated for 1 hour prior to purification of the complex by size exclusion chromatography into 20 mM HEPES pH 7.5, 150 mM NaCl using a Superdex 75 10/300 column (GE Healthcare Life Sciences). Crystallisation trials were carried out using vapour diffusion in sitting drops by mixing 100 nl of protein solution with 100 nl of well solution. Crystals were obtained after 10 days with a well solution of 200 mM ammonium acetate, 100 mM HEPES pH 7.5, 25 % v/v isopropanol. These were cryoprotected by transfer into drops of well solution supplemented with 25% MPD, and were cryo-cooled for data collection in liquid nitrogen.

Data were collected at the Proxima-1 beamline at SOLEIL at a wavelength of 0.97857 Å. Data were then indexed using DIALS (v3.0)²¹, and scaled using AIMLESS (v0.73)²², giving a complete dataset at a resolution of 3.0 Å. The structure was solved by molecular replacement using Phaser MR (v2.8.3)²³, with the individual domains of LILRB1 (from PDB codes 6EWA and 4LL9) used as four separate search models. The model was built and refined using cycles of COOT (v0.8.9.2)²⁴ and BUSTER (v2.10)²⁵.

Sequence analysis

We extracted 185 RIFIN amino acid sequences from the *Plasmodium falciparum* 3D7 v3.2 genome assembly²⁶. These were aligned using MUSCLE v3.8.31 with default parameters²⁷. Sequence LOGOs were generated using <http://weblogo.threeplusone.com>²⁸.

Circular dichroism

Circular dichroism experiments were conducted using a Jasco J815 CD Spectrophotometer. The proteins were desalted into 20 mM sodium phosphate pH 7.5, 150 mM NaF buffer using PD-10 columns (GE Healthcare), and were adjusted to a concentration of 0.25 mg ml⁻¹. A spectrum was taken at 20°C between 260 nm and 190 nm using a 1 mm path length, with measurements taken every 0.5 nm. A baseline determined using buffer alone was subtracted from the protein spectra and ten equivalent spectra were averaged together.

Surface plasmon resonance

Surface plasmon resonance experiments were carried out using a Biacore T200 instrument (GE Healthcare Life Sciences). LILRB1 constructs (D1D4, D1D2, and D3D4) were coupled to a CM5 chip by amine coupling. Concentration series of RIFIN constructs were flowed over this chip at 30 µl/min, with a 240 s contact time, and a 240 s dissociation time. After each run the chip was regenerated using 10 mM glycine pH 2.5 for 30 s. All experiments were carried out using 20 mM Hepes pH 7.5, 150 mM NaCl, 0.005% Tween-20 and data

were analysed using the BiaEvaluation software (v1.0) to conduct kinetic analysis and Prism (v8.2.1) for equilibrium analysis.

GFP reporter assay

The GFP reporter assay was conducted as described^{5,29}. The LILRB1 reporter cells were mouse T cell hybridomas that were stably transfected with NFAT-GFP, FLAG-tagged DAP12 and a fusion of the extracellular domain of LILRB1 with the transmembrane and intracellular domains of paired immunoglobulin-like receptor β (PILRP). The transmembrane and cytoplasmic domains of PILRP were used to induce GFP via the DAP12 adaptor molecule in the reporter cells. Recombinant RIFINs (at 0.3, 1, 3, 10 or 30 $\mu\text{g ml}^{-1}$) were immobilized on a 96-well plate. PF3D7_1254200 is the same as RIFIN #5 in Saito et al 2017. Its folding was assessed by circular dichroism analysis⁵. LILRB1 reporter cells and control reporter cells were cultured on the RIFIN-immobilized plate at 1×10^5 cells per well for 16 h. GFP expression was analysed using flow cytometry.

Plasmodium falciparum parasite culture and transfections

Plasmodium falciparum strain 3D7 was cultured with human red blood cells (type O blood, hematocrit (Ht) 2%, the Japanese Red Cross Blood Center) in RPMI-1640 containing 10% human serum, 20% AlbuMAX I (Life Technologies), 25mM HEPES, 0.225% sodium bicarbonate and 0.38 mM hypoxanthine supplemented with $10\mu\text{g ml}^{-1}$ gentamicin. Parasites were incubated in an atmosphere containing 90% N_2 , 5% CO_2 and 5% O_2 . 5% D-sorbitol and Percoll density gradient centrifugation (GE Healthcare) were used to maintain synchronous cultures. Without selection, the 3D7 parasite will be expressing a mixture of RIFINs and do not show appreciable binding to LILRB1⁵. Transgenic parasites were generated as previously described^{5,30}. Two biologically independent lines were prepared for each mutant and the parasites were grown in RPMI-1640 containing 25ng ml^{-1} pyrimethamine.

Flow cytometry to assess LILRB1 binding by infected erythrocytes

A plasmid for expression of LILRB1-Fc fusion protein was constructed as previously described³¹. LILRB1-Fc was prepared by transient transfection of HEK293T cells using PEI Max (Polysciences) and its binding to infected erythrocytes was evaluated as previously described⁵. In brief, trophozoite- and schizont-stage parasites were stained with $10\mu\text{g ml}^{-1}$ LILRB1-Fc premixed with an allophycocyanin (APC)-conjugated anti-human IgG Fc antibody (109-136-098, Jackson ImmunoResearch Laboratories, diluted 1:100). The LILRA2-Fc fusion protein was used as a control. Flow cytometric analysis was conducted using a BD FACSVerser flow cytometer (BD Biosciences). Data were analysed using FlowJo software (FlowJo; v10.4).

Flow cytometry to assess LILRB1 expression

Peripheral white blood cells were obtained from leukocyte cones provided by UK National Health Service Blood and Transplant. Use of leukapheresis products at the University of Oxford was approved by the Non-Clinical Issue division of the National Health Service (REC 11/H/11/7). Informed consent was obtained by NHSBT upon donation and the identity

of the donor was not disclosed. Cells were fixed with 4% paraformaldehyde (ThermoFisher Scientific, 28908) for 10 minutes, then washed with phosphate buffered saline (PBS) and incubated overnight with Human TruStain FcX (BioLegend, 422302) to block non-specific Fc- receptor binding. Staining was performed at 4°C in PBS with 0.1% sodium azide. The following antibodies were used to identify lymphocyte and granulocyte subsets: PE-Cy5 anti-CD3 (UCHT1; BioLegend), BV-421 anti-TCR β (IP26; BioLegend), APC-Cy7 anti-CD4 (OKT4; BioLegend), PE anti-CD25 (2A3; BD Biosciences), Alexa Fluor 488 anti-CXCR5 (RF8B2; BD Biosciences), APC-Cy7 anti-CD19 (HIB19; BioLegend), PE anti-CD20 (2H7; BioLegend), BV421 anti-CD38 (HIT2; BioLegend), PerCP anti-HLA-DR (L243; BioLegend), APC-Cy7 anti-CD11c (Bu15; BioLegend), PE anti-CD123 (6H6; BioLegend) and Alexa Fluor 488 anti-CD56 (HCD56; BioLegend). Finally, samples were stained with rabbit anti-LILRB1 (abcam, EPR21007) followed by Alexa Fluor 647-conjugated F(ab)'2 anti-rabbit (ThermoFisher Scientific, A-27040). All primary antibodies were used at a working dilution of 5 μ l per 10⁶ leukocytes and the secondary F(ab)'2 was used at a concentration of 2 μ g ml⁻¹. Compensation was performed with single colour controls. Data were collected on a BD LSRFortessa X-20 (BD Biosciences), running BD FACSDiva software (v6.0), and analysed using FlowJo software (v10.4). LILRB1 expression levels on select leukocyte subsets were calculated by gating on LILRB1+ cells and fluorescence intensity converted to absolute protein numbers by reference to Quantum Alexa Fluor 647 MESF calibration beads (Bangs Laboratories) assuming an antibody:antigen labelling ratio of 1.

T cell subsets were gated as follows: $\alpha\beta$ negative (CD3+ $\alpha\beta$ TCR⁻), CD8+ (CD3+ $\alpha\beta$ TCR+ CD4⁻), TH (CD3+ $\alpha\beta$ TCR+ CD4+ CD25^{low} CXCR5⁻), TFH (CD3+ $\alpha\beta$ TCR+ CD4+ CD25^{low} CXCR5⁺), and Treg (CD3+ $\alpha\beta$ TCR+ CD4+ CD25^{high} CXCR5⁻). B cell subsets were gated as follows: effector (CD19+ CD20+ CD38⁺), memory (CD19+ CD20+ CD38⁻), and plasmablasts (CD19+ CD20⁻). Granulocyte subsets were gated as follows: basophils (HLA-DR^{low} CD123⁺), neutrophils (HLA-DR^{med}CD11c^{med}), and DC/macrophages (HLA-DR^{high} CD11c^{high}). Other lymphocytes were gated as follows: NK (CD56⁺ CD3⁻), and NKT (CD56⁺ CD3⁺). Monocytes were gated based on forward/side scatter profile. Gating strategies are illustrated in Supplementary Figure 2.

NK cell isolation

Primary human NK cells were isolated from peripheral blood cones obtained from the UK National Health Service Blood and Transplant, as described above. Cells from three donors were isolated using the RosetteSepTM Human NK Cell Enrichment Cocktail (StemCell Technologies). Isolated cells were resuspended in RPMI-1640 supplemented with 2 mM L-glutamine, 10 mM HEPES, and 1% penicillin-streptomycin solution (GIBCO) at 37°C and were used for imaging experiments on the same day.

Supported Lipid Bilayer preparation

Supported lipid bilayers (SLBs) were prepared as described previously³². Briefly, micelles of 1,2-dioleoyl-sn-glycero-3-phosphocholine (Avanti Polar Lipids) supplemented with 12.5% 1,2-dioleoyl-sn-glycero-3-[(N-(5-amino-1-carboxypentyl)iminodiacetic acid)succinyl]-Ni (Avanti Polar Lipids) were flowed onto plasma cleaned glass coverslips affixed

with adhesive 6-lane chambers (ibidi). SLBs were blocked with 5% filtered casein, washed 3x in PBS and incubated with recombinant His-tagged proteins of interest. These were produced in-house, with the exception of pMHC, which is HLA-A2 loaded with 1G4-TCR specific NY-ESO peptide, and was a gift from Edward Jenkins and Simon Davis, University of Oxford. pMHC, RIFIN and G234R were conjugated to Alexa Fluor 647 by succinimidyl ester-mediated labeling of primary amines (ThermoFisher Scientific, A20186) to achieve 1-2 fluorophore molecules per protein molecule. The coupling of labelled proteins to SLBs was calibrated using a bead-supported lipid bilayer system. In short, Quantum Alexa Fluor 647 MESF calibration beads (Bangs Laboratories) of a known diameter were used to relate fluorescence intensity to fluorophore density and allowed the calibration of protein concentrations to bilayer densities (see Extended Data Figure 7). These calibration curves were used to infuse equivalent densities of pMHC, RIFIN and G234R onto SLBs which was further verified by acquiring images of equivalent homogenous fluorescence (data not shown). The final densities used were: 600 molecules/ μm^2 for ICAM1 and 100 molecules/ μm^2 for pMHC, RIFIN and G234R. The human PFRH5-targeting R5.016 antibody³³ (IgG1) was coupled to the SLBs using His-tagged PFRH5 at a concentration of 100 nM.

Within two hours of preparation, SLBs were pre-warmed to 37°C and $\sim 1 \times 10^6$ primary NK cells were infused into each lane. Samples were incubated for 30 min at 37°C/5% CO₂ then fixed with warm 4% paraformaldehyde in PHEM (60 mM PIPES, 25 mM HEPES, 10 mM EGTA, 2 mM MgCl₂, pH 7.4) for 15 minutes before washing 3x with PHEM. Each lane was permeabilised with 0.1% saponin in PHEM buffer for 20 min, then washed and blocked with 100 mM glycine/5% BSA in PHEM for 16 hr. For perforin staining, a monoclonal antibody to perforin conjugated to Alexa Fluor 488 (BioLegend, dG9) was diluted in PHEM buffer with 0.02% saponin, 3% BSA and added to samples for 1 h before washing 5x with PHEM buffer prior to imaging. For LILRB1 staining, two non-blocking primary monoclonal rabbit antibodies to LILRB1 (abcam, EPR21007 and EPR11256) were diluted in PHEM buffer containing 0.02% saponin, 3% BSA and added to samples for 1 h before washing. To reduce background staining, goat anti-rabbit F(ab')₂ conjugated to Alexa Fluor 568 (ThermoFisher Scientific, A-21069) was diluted in 0.02% saponin, 10% human serum for 20 minutes before being added to samples for 1 h. Finally, samples were washed 5x with PHEM buffer prior to imaging.

TIRF microscopy and image analysis

Imaging was performed on an Olympus cell TIRF-4Line system, with cellSENS Dimension software (v2.3) using a 150x (NA 1.45) oil objective at room temperature. Image analysis was performed using ImageJ (v.1.52p, NIH). Cell-boundaries were defined based on segmented ('Default' algorithm in ImageJ) reflection images and all pixels in the contact area used to calculate the mean fluorescence intensity (MFI). Pearson's correlation coefficient (PCC) values were calculated for each cell contact using the Coloc2 plugin to perform pixel intensity correlations between channels.

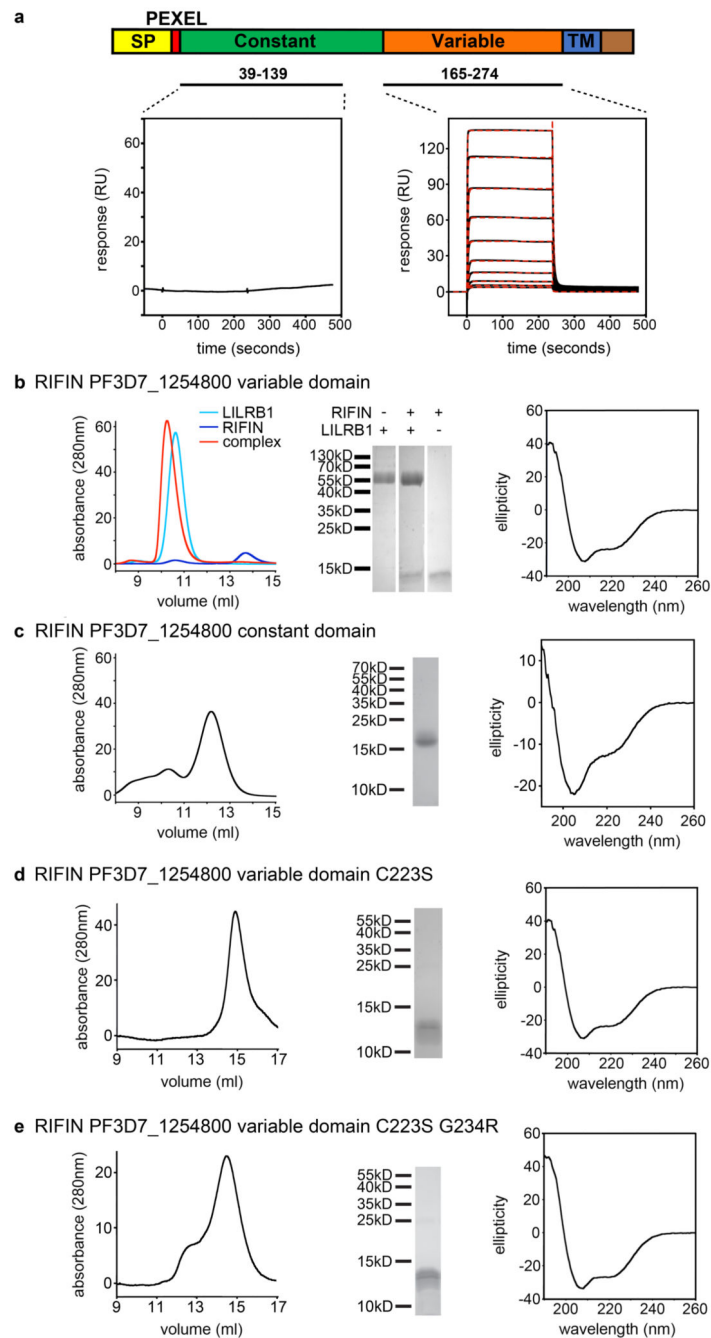
Statistics

MFI values for pMHC/RIFIN/G234R recruitment were normalised to the background bilayer fluorescence in each condition to account for differences in labelling and coupling

efficiency. MFI values for perforin mobilisation were normalised to the minimum value in each condition to account for differences in cellular auto-fluorescence between donors. The non-normalised MFI values coloured by donor are included in Extended Data Figure 8.

Fluorescence intensity and correlation values from each donor were pooled and analysed statistically using GraphPad Prism (v8.2.1) software. Samples were tested for normality with a D'Agostino-Pearson test. For normally distributed data significance was assessed with a one-way analysis of variance (ANOVA) followed by Tukey's post hoc test. Otherwise, significance was measured with a ranked Kruskal-Wallis test followed by Dunn's test for multiple comparisons. Significance was defined as $p < 0.05$ (* $p < 0.05$, ** $p < 0.01$, *** $p < 0.001$, **** $p < 0.0001$) and non-significant comparisons are not shown. In figure 3e Tukey's test was performed on the following sample sizes: control ($n = 80$), pMHC ($n = 84$), RIFIN ($n = 104$), and G234R ($n = 78$). All comparisons had an adjusted p value < 0.0001 except for control versus G234R ($p = 0.03$). In figure 3f, Tukey's test was performed on the following sample sizes: pMHC ($n = 61$), RIFIN ($n = 65$), and G234R ($n = 71$). All comparisons had an adjusted p value < 0.0001 . In figure 3g, Dunn's test was performed on the following sample sizes: control ($n = 80$), pMHC ($n = 84$), RIFIN ($n = 104$), and G234R ($n = 78$). All comparisons had an adjusted p value < 0.0001 except for control vs pMHC ($p = 0.04$), while control versus G234R and pMHC versus RIFIN were non-significant ($p > 0.9999$).

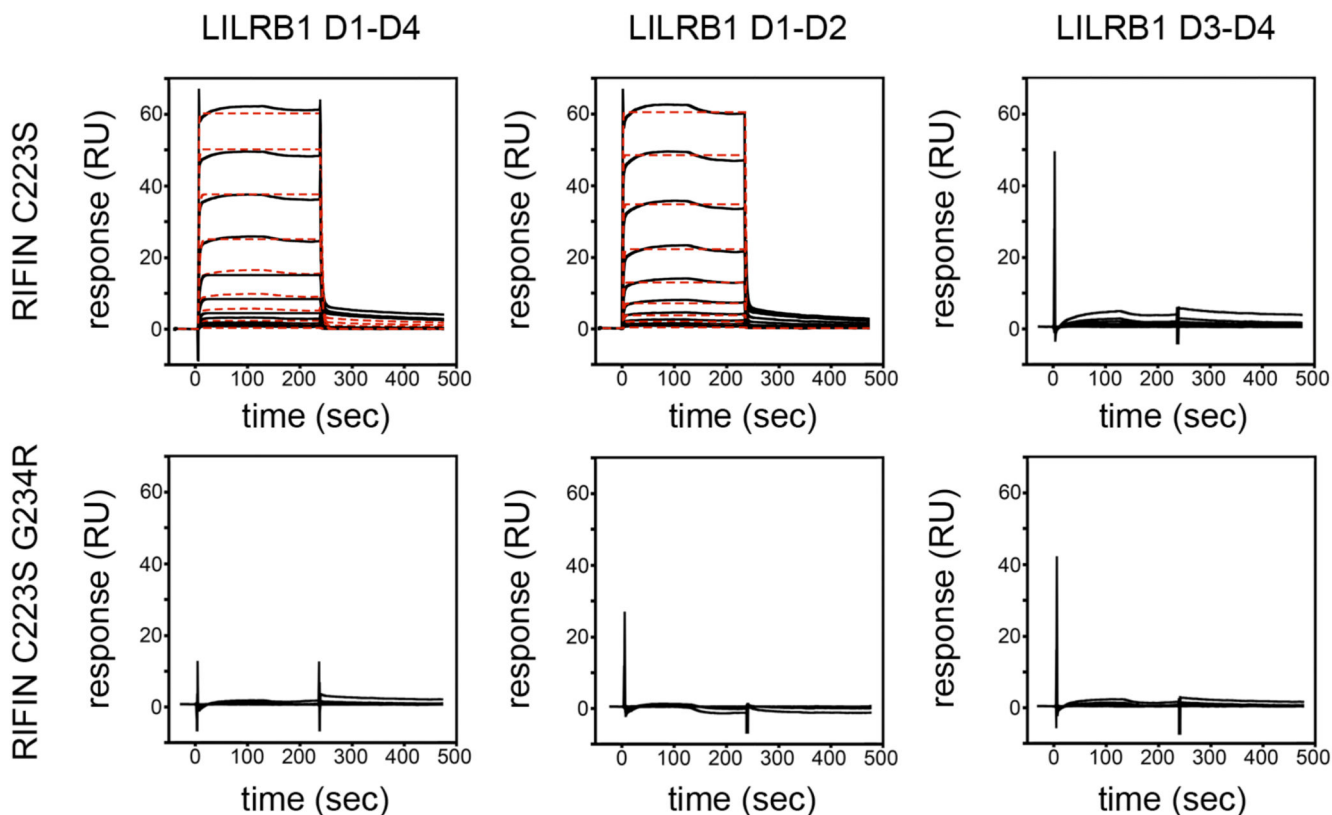
Extended Data



Extended Data Figure 1. Biophysical characterisation of RIFIN variable and constant regions, and the RIFIN:LILRB1 complex.

a. Schematic showing the domain architecture of a RIFIN, using numbering from PF3D7_1254800, and surface plasmon resonance analysis of the binding of the PF3D7_1254800 constant and variable regions to immobilised LILRB1. The variable region was injected in a two-fold dilution series from 4 μ M to 3.9nM, while a single injection of 4 μ M was used for the constant region. Equilibrium fitting gave $K_D=570 \pm 130$ nM. Red

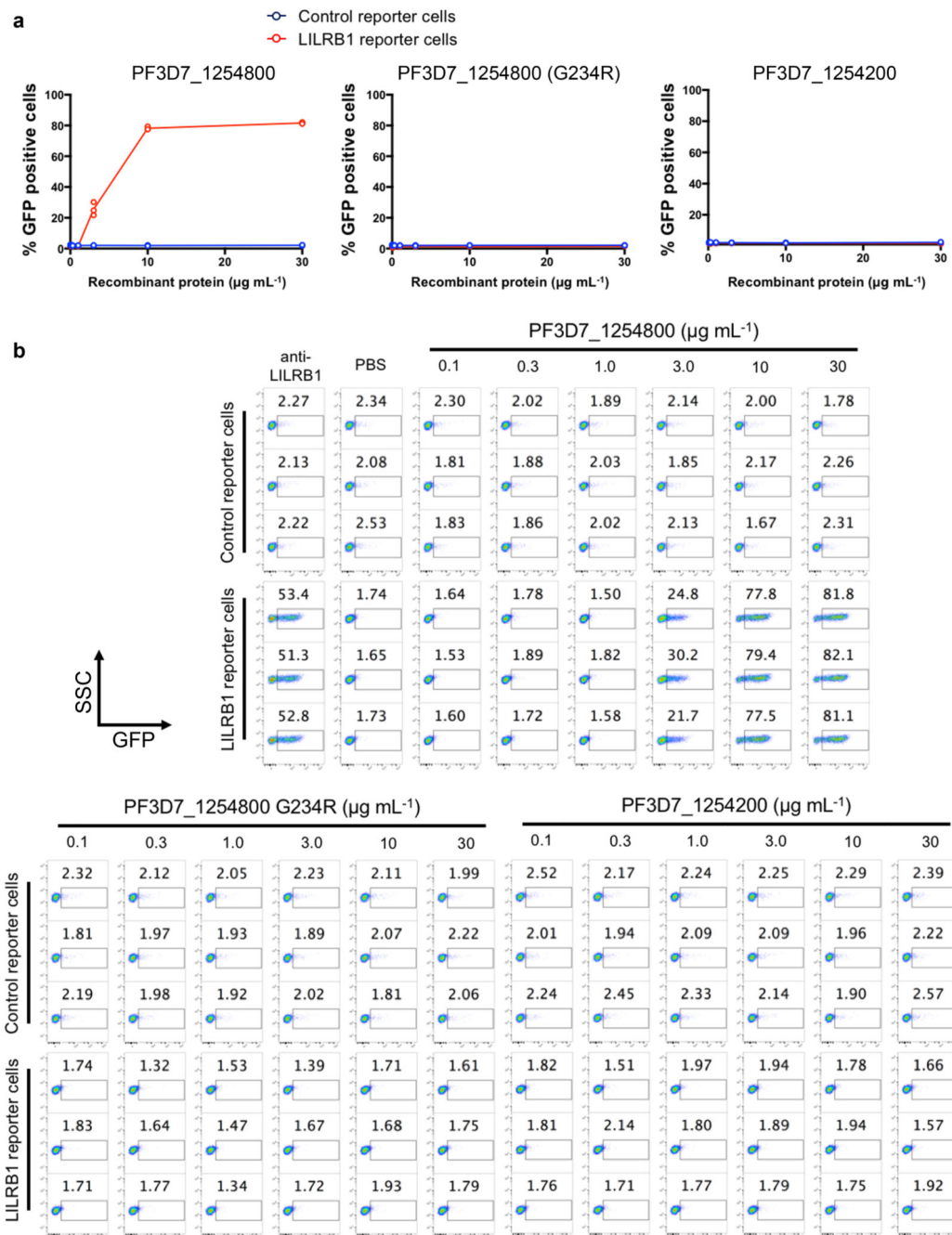
dotted lines show the fitting to a one-to-one kinetic binding model and give $K_D=1.13\mu\text{M}$, $k_a=2.63\times 10^5\text{M}^{-1}\text{s}^{-1}$ and $k_d=0.297\text{ s}^{-1}$ ($\chi^2=3.88\text{RU}^2$) with $n=1$ for each series. **b.** Size exclusion chromatograms and Coomassie-stained SDS-PAGE gel showing LILRB1 ectodomain, RIFIN 1254800 variable region and their complex, and a circular dichroism spectrum for the RIFIN. **c.** Size exclusion chromatogram, Coomassie-stained SDS-PAGE gel, and circular dichroism spectrum for the RIFIN 1254800 constant region. **d.** Size exclusion chromatogram, Coomassie-stained SDS-PAGE gel, and circular dichroism spectrum for the RIFIN PF3D7_1254800 C223S mutant. **e.** Size exclusion chromatogram, Coomassie-stained SDS-PAGE gel, and circular dichroism spectrum for the RIFIN PF3D7_1254800 C223S G234R mutant. Circular dichroism data shows the average of ten technical replicates, while size exclusion chromatograms and gels are from single experiments



Extended Data Figure 2. Surface plasmon resonance analysis of RiFiN binding to LILRB1.

Surface plasmon resonance analysis of the binding of RIFIN PF3D7_1254800 variable region containing mutations C223S or C223S G234R to different LILRB1 constructs, showing that the RIFIN binding site is contained within domains 1 and 2 of LILRB1 and involves RIFIN residue G234. Each RIFIN was injected in a two-fold dilution series from $4\mu\text{M}$ to 3.9nM . For binding to D1-D4, equilibrium fitting gave $K_D = 700 \pm 5\text{ nM}$. Red dotted lines show the fitting to a one-to-one kinetic binding model and give $K_D=1.04\mu\text{M}$, $k_a=2.88\times 10^5\text{M}^{-1}\text{s}^{-1}$ and $k_d=0.299\text{ s}^{-1}$ ($\chi^2=3.76\text{RU}^2$) with $n=1$ for each series. For binding to D1-D2, equilibrium fitting gave $K_D= 1.10 \pm 0.05\ \mu\text{M}$. Red dotted lines show the fitting to

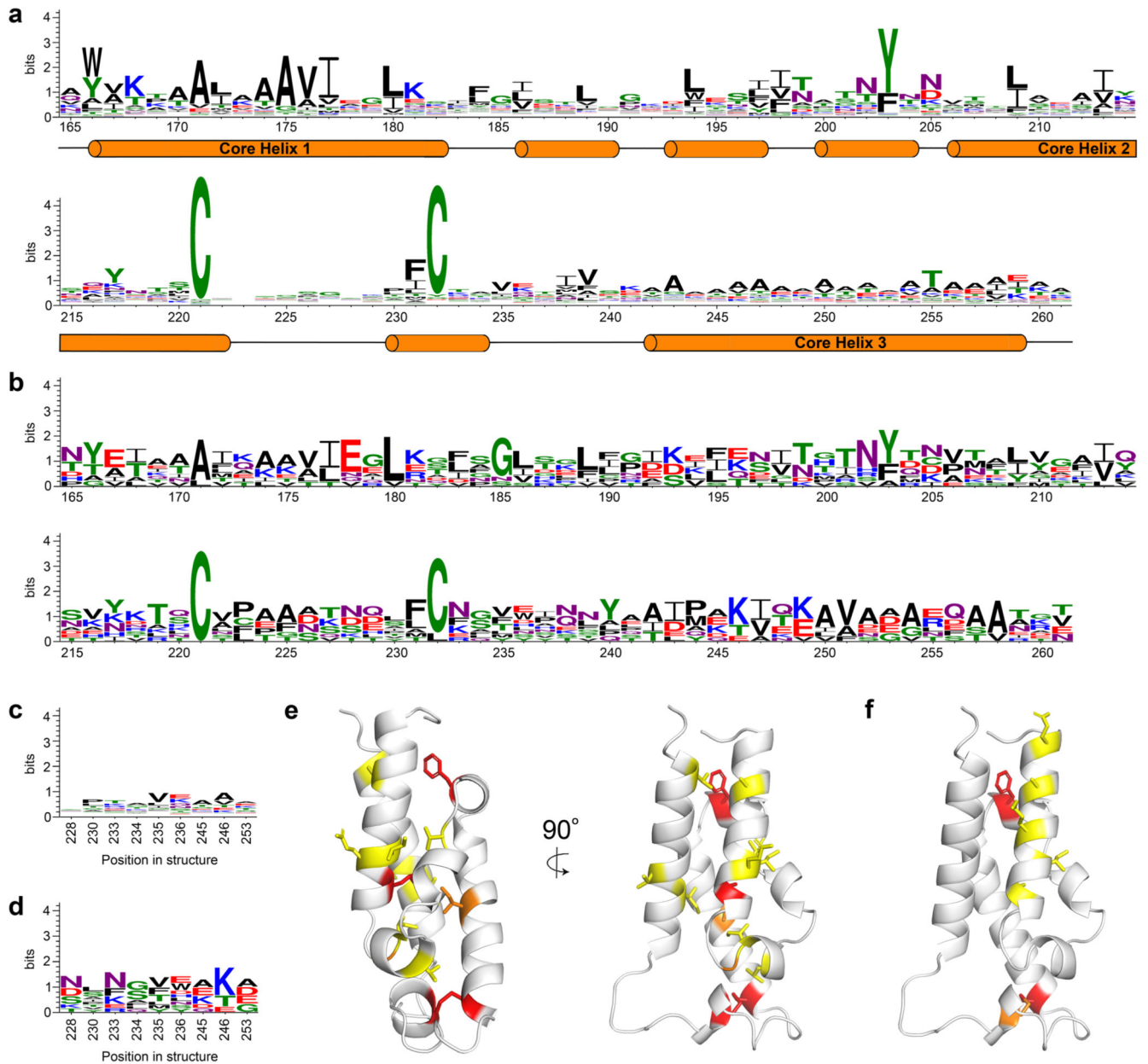
a one-to-one kinetic binding model and give $K_D=1.33\mu\text{M}$, $k_a=4.37\times 10^5\text{M}^{-1}\text{s}^{-1}$ and $k_d=0.579\text{s}^{-1}$ ($\chi^2=4.04\text{RU}^2$) with $n=1$ for each series.



Extended Data Figure 3. Analysis of the effect of RIFINs on signalling in a T cell based GFP report system.

a. NFAT-GFP-based reporter system which expresses GFP in response to LILRB1-mediated signalling was used to assess the effect of RIFINs. Fluorescent signalling of the LILRB1-reporter cells and control reporter cells were assessed in triplicate in the presence of the immobilized LILRB1-binding RIFIN variable domain (PF3D7_1254800: C223S), its

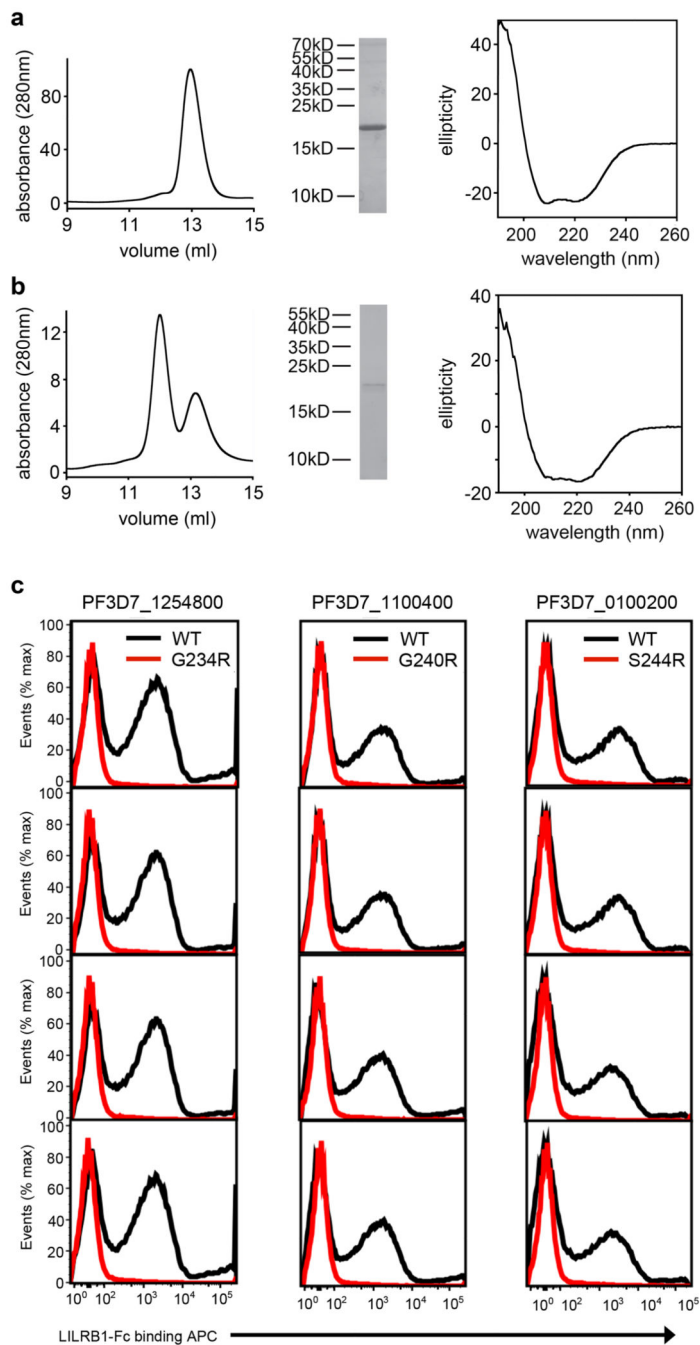
G234R mutant (C223S G234R) and a RIFIN which does not bind LILRB1 (PF3D7_1254200). **b.** Flow cytometry images used to derive a.



Extended Data Figure 4. Analysis of the sequence variability of RIFINs.

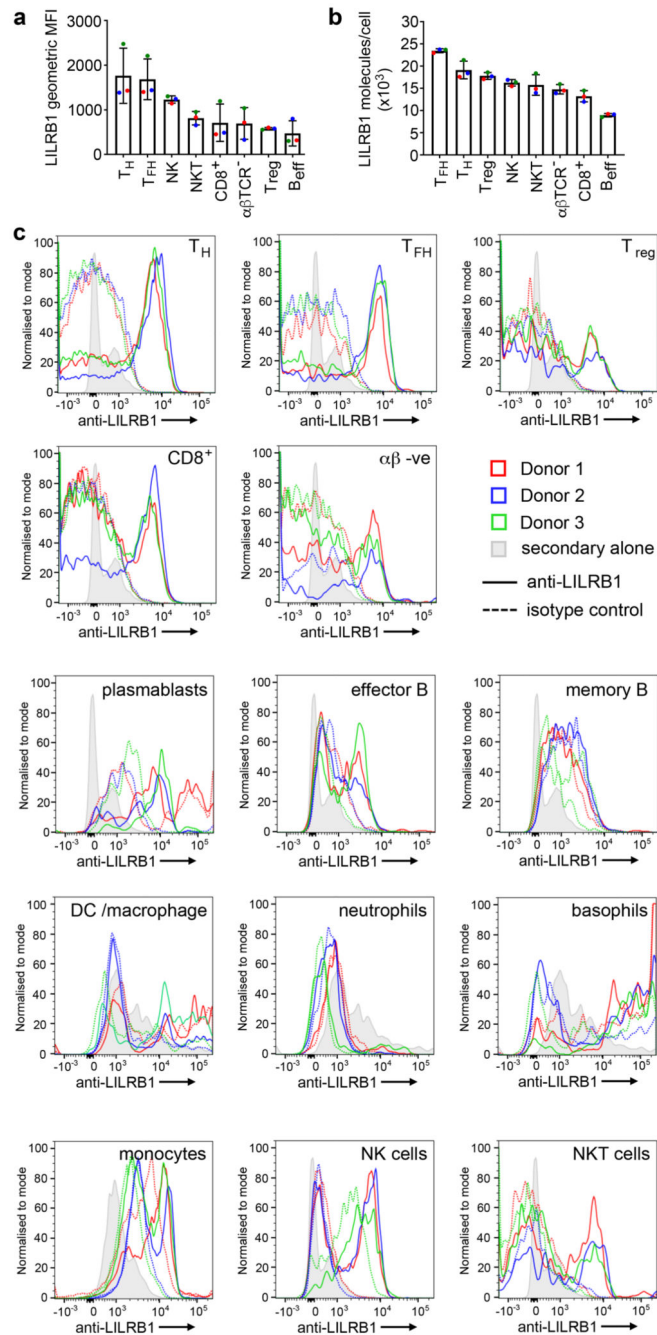
a. A sequence LOGO for 185 RIFINs from the 3D7 strain of *Plasmodium falciparum*. Numbers are those from the 1254800 RIFIN and the orange cylinders beneath the numbers represent the positions of helices in the RIFIN structure. **b.** An equivalent sequence LOGO for ten LILRB1-binding RIFINs. **c.** and **d.** Sequence LOGOs for the residues which in PF3D7_1254800 contact LILRB1 in **c.** 185 RIFINs from 3D7 and **d.** 10 LILRB1-binding RIFINs. **e.** The structure of the RIFIN with the most conserved residues in ten LILRB1-binding RIFINs coloured. Red represents a sequence entropy of <0.5 ; orange is 0.5-0.75 and

yellow is 0.75-1.0. **f.** An equivalent representation of conserved residues across 185 RIFINs from 3D7.



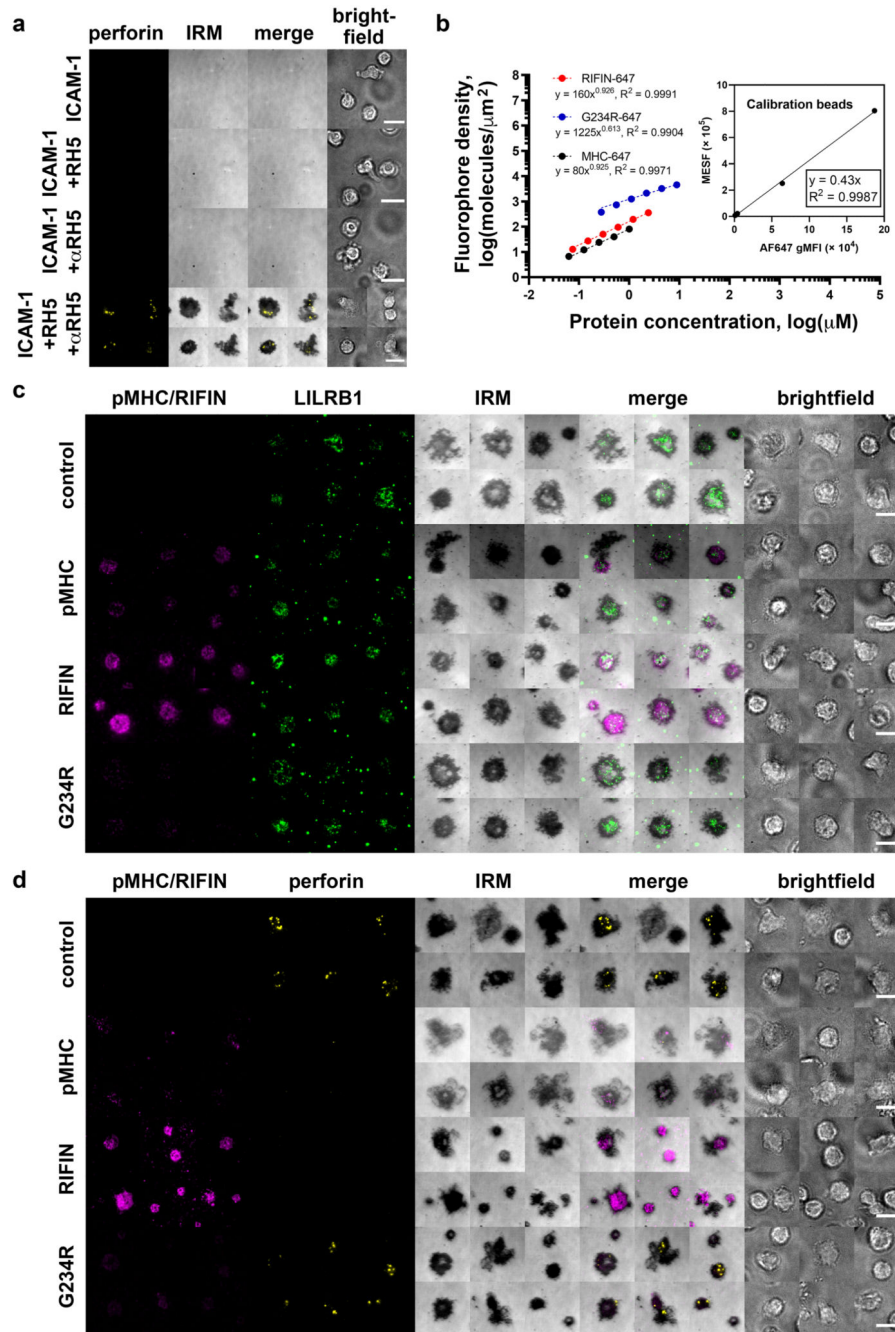
Extended Data Figure 5. Analysis of the effect of point mutations on LILRB1-binding by RIFINs
a. Size exclusion chromatogram, Coomassie-stained SDS-PAGE gel, and circular dichroism spectrum for the PF3D7_0100400 variable region. **b.** Size exclusion chromatogram, Coomassie-stained SDS-PAGE gel, and circular dichroism spectrum for the PF3D7_0100400 variable region with the L264R mutation. The peak at ~13.3ml

corresponded to monomer, with the same mobility observed for PF3D7_0100400 and was used for subsequent experiments. Circular dichroism data shows the average of ten technical replicates, while size exclusion chromatograms and gels are from single experiments. **c.** Flow cytometry analysis of the binding of LILRB1-Fc to erythrocytes infected with transgenic parasites expressing specific RIFINs.



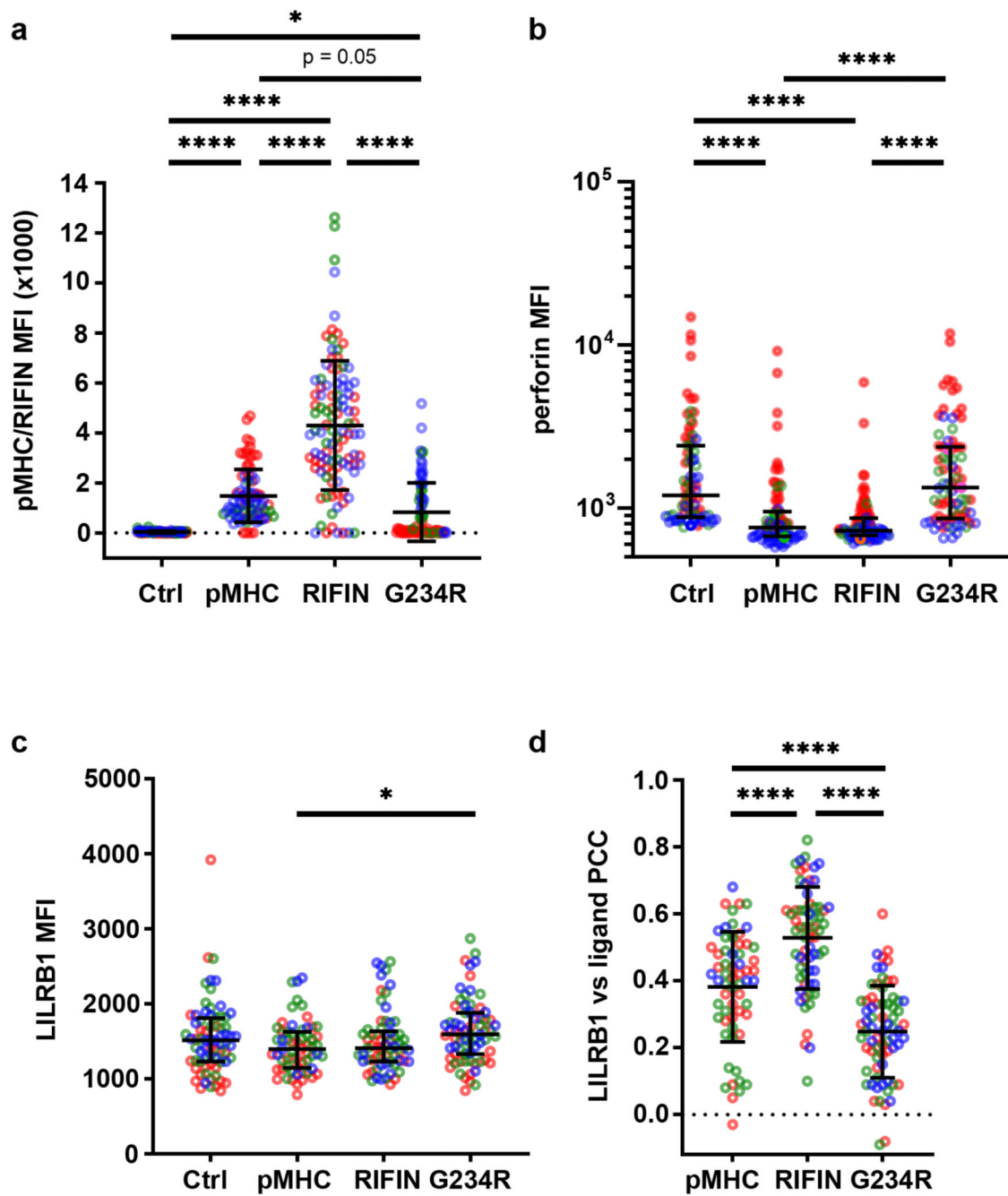
Extended Data Figure 6. Measurement of quantities of LILRB1 on different plasma white blood cells after fluorescent sorting.

a. Summary of LILRB1 expression levels on select leukocyte subsets. **b.** LILRB1 surface densities were calculated using MESF calibration beads as described in the Methods section. **c.** Original histograms on which these measurements are based. In figures 3a and 3b, error bars are represented as mean \pm 1 SD. Each circle represents the measurement from one donor. T_h = helper T cell, T_{fh} = follicular helper T cell, T_{reg} = regulatory T cell, B_{eff} = effector B cell, NKT = natural killer T cell. In all panels, data was collected for three independent donors, colour coded as in panel c.



Extended Data Figure 7. Imaging LILRB1 and perforin in an NK cell immunological synapse model

a. PFRH5 and anti-PFRH5 R5.016 antibody (aRH5), together with ICAM-1, trigger NK cell contact formation and perforin (yellow) mobilisation to the synapse. Representative images are shown from one of two independent experiments with similar results. **b.** A calibration curve for the density of pMHC, RIFIN (C223S) and G234R (C223S G234R) on SLBs. **c.** Supplementary images of LILRB1 localisation (green) in NK cells in the contact area on SLBs coated with RIFIN, G234R mutant or MHC class I (pMHC) (magenta). **d.** Supplementary images of perforin mobilisation (yellow) in NK cells on SLBs coated with RIFIN, G234R mutant or MHC class I (pMHC) (magenta). Scale bars = 10 μm . Three independent experiments were carried out with cells from different donors with similar results. The raw MFI values of these experiments are shown in ED figure 8a, 8b and 8c.



Extended Data Figure 8. analysis of quantity and co-localisation of RIFIN and its G234R mutant, pMHC, LILRB1 and perforin at the NK cell immunological synapse

Fluorescence measurements from three donors, each indicated by a different colour, were analysed to investigate: **a.** the quantity of RIFIN (C223S), G234R (C223S G234R) and pMHC at the contact area; **b.** perforin mobilisation to the synapse under each condition; **c.** the quantity of LILRB1 at the contact area and; **d.** the degree of co-localisation of RIFIN, G234R and pMHC with LILRB1. In figure 8a, Tukey's post hoc test was performed on the following sample sizes: control (n = 80), pMHC (n = 84), RIFIN (n = 104), G234R (n = 78).

All comparisons had an adjusted p value < 0.0001 except for control versus G234R ($p = 0.01$) and pMHC vs G234R (shown). In figure 8b, Dunn's test was performed on the following sample sizes: control ($n = 80$), pMHC ($n = 84$), RIFIN ($n = 104$), G234R ($n = 78$). All comparisons had an adjusted p value < 0.0001 except for control versus G234R and pMHC vs RIFIN which were non-significant ($p > 0.9999$). In figure 8c, Dunn's test was performed on the following sample sizes: control ($n = 72$), pMHC ($n = 61$), RIFIN ($n = 65$), G234R ($n = 71$)

All comparisons were highly non-significant ($p > 0.9999$) except for control vs G234R ($p = 0.64$), RIFIN vs G234R ($p = 0.18$) and MHC vs G234R ($p = 0.02$). Figure 8d is identical to figure 3f but with each measurement colour-coded by donor. Tukey's post hoc test was performed on the following sample sizes: RIFIN ($n=65$ cells), G234R ($n=71$ cells) and pMHC ($n=61$ cells). All had adjusted p value < 0.0001 . Data are represented as mean \pm 1 SD for figures 8a and 8d and median \pm interquartile range for figures 8b and 8c. For further details of statistical testing, see the Methods section.

Extended Data Table 1
Crystallographic analysis of the RIFIN:LILRB1 complex

RIFIN variable region -LILRB1 D1-D4	
Data collection	
Space group	P6 ₁ 2 2
Cell dimensions	
a, b, c (Å)	134.51, 134.51, 277.47
α , β , γ (°)	90, 90, 120
Wavelength	0.97857 Å
Resolution (Å)	277.47 – 3.00 (3.16 – 3.00)
Total Observations	602390 (89498)
Total Unique	30613 (4346)
R_{pim} (%)	6.5 (64.7)
CC _{1/2}	0.99 (0.76)
$I/\sigma(I)$	9.4 (1.6)
Completeness (%)	100.0 (100.0)
Multiplicity	19.7 (20.6)
Wilson B factor	90.83
Refinement	
Reflections	30517
R_{work} / R_{free} (%)	23.40/24.87
Average B factor	
Protein	119.6
Glycans	176.0
Number of residues	
Protein	496
Glycans	4

R.m.s deviations	
Bond lengths (Å)	0.011
Bond angles (°)	1.25
Ramachandran plot	
Favored (%)	93.8
Allowed (%)	6.2
Outliers (%)	0.0

Extended Data Table S2
interactions between the RIFIN and LILRB1

RIFIN (1254800 Variable Region)		LILRB1-FL		
Residue	Group	Residue	Group	Interaction Type
N228	Side chain NH ₂	Q125	Backbone O	Hydrogen bond
L230	Side chain	Y99	Side chain	Hydrophobic
		V126	Side chain	Hydrophobic
		F128	Side chain	Hydrophobic
R233	Side chain N	Q125	Side chain O	Hydrogen bond
G234	Backbone O	I100	Backbone NH	Hydrogen bond
M235	Side chain	Y99	Side chain	Hydrophobic
N236	Side chain NH ₂	G97	Backbone O	Hydrogen bond
	Backbone NH	A98	Backbone O	Hydrogen bond
K245	Side chain NH ₂	E68	Side chain OH	Hydrogen bond
K246	Side chain NH ₂	E184	Side chain OH	Hydrogen bond
E253	Side chain OH	K42	Side chain NH ₂	Hydrogen bond

Supplementary Material

Refer to Web version on PubMed Central for supplementary material.

Acknowledgements

MKH is funded by a Wellcome Investigator Award (101020/Z/13/Z). TEH is funded by the Peter J. Braam graduate scholarship for Global Wellbeing at Merton College, Oxford. AMM is funded by the Wellcome Trust PhD Studentship in Science (108869/Z/15/Z). JHF is a Wellcome Trust Sir Henry Wellcome Fellow (107375/Z/15/Z). MLD is a Wellcome Trust Principal Research Fellow (100262Z/12/Z). HA is funded by JSPS KAKENHI (JP 18H05279, 19H04808) and AMED J-PRIDE (19fm0208004h0003). AS is supported by a JSPS Research Fellowship for Young Scientists (18J20300). AJR is funded by the Wellcome Trust (206194/Z/17/Z) and the Medical Research Council (Programme grant: MR/M003906/1). The authors thank Ed Lowe and the staff at beamline Promixa1 at Soleil for help with crystallographic data collection, David Staunton for help with biophysical analysis, Simon Davis and Edward Jenkins for supplying recombinant pMHC-His, Prof. Toshihiro Hori for *P. falciparum* culture and Prof. Shiro Iwanaga for generation of RIFIN-transgenic *P. falciparum*.

Data Availability

Coordinates and structure factors are available from the Protein Data Bank with accession code 6ZDX. All biophysical and imaging data is provided as Source Data while flow data is

deposited at FigShare <https://doi.org/10.6084/m9.figshare.c.5025038.v1>. Any queries should be addressed to the corresponding author.

References

1. Chan JA, Fowkes FJ, Beeson JG. Surface antigens of *Plasmodium falciparum*- infected erythrocytes as immune targets and malaria vaccine candidates. *Cell Mol Life Sci.* 2014; 71:3633–57. [PubMed: 24691798]
2. Tan J, et al. A LAIR1 insertion generates broadly reactive antibodies against malaria variant antigens. *Nature.* 2016; 529:105–9. [PubMed: 26700814]
3. Pieper K, et al. Public antibodies to malaria antigens generated by two LAIR1 insertion modalities. *Nature.* 2017; 548:597–601. [PubMed: 28847005]
4. Hsieh FL, Higgins MK. The structure of a LAIR1-containing human antibody reveals a novel mechanism of antigen recognition. *Elife.* 2017; 6
5. Saito F, et al. Immune evasion of *Plasmodium falciparum* by RIFIN via inhibitory receptors. *Nature.* 2017; 552:101–105. [PubMed: 29186116]
6. Bachmann A, et al. A comparative study of the localization and membrane topology of members of the RIFIN, STEVOR and PfMC-2TM protein families in *Plasmodium falciparum*-infected erythrocytes. *Malar J.* 2015; 14:274. [PubMed: 26173856]
7. Goel S, et al. RIFINs are adhesins implicated in severe *Plasmodium falciparum* malaria. *Nat Med.* 2015; 21:314–7. [PubMed: 25751816]
8. Wang Q, et al. Structures of the four Ig-like domain LILRB2 and the four-domain LILRB1 and HLA-G1 complex. *Cell Mol Immunol.* 2019
9. Nam G, et al. Crystal structures of the two membrane-proximal Ig-like domains (D3D4) of LILRB1/B2: alternative models for their involvement in peptide-HLA binding. *Protein Cell.* 2013; 4:761–70. [PubMed: 23955630]
10. Willcox BE, Thomas LM, Bjorkman PJ. Crystal structure of HLA-A2 bound to LIR-1, a host and viral major histocompatibility complex receptor. *Nat Immunol.* 2003; 4:913–9. [PubMed: 12897781]
11. Higgins MK, Carrington M. Sequence variation and structural conservation allows development of novel function and immune evasion in parasite surface protein families. *Protein Sci.* 2014; 23:354–65. [PubMed: 24442723]
12. Chapman TL, Heikema AP, West AP Jr, Bjorkman PJ. Crystal structure and ligand binding properties of the DID2 region of the inhibitory receptor LIR-1 (ILT2). *Immunity.* 2000; 13:727–36. [PubMed: 11114384]
13. Hsieh FL, et al. The structural basis for CD36 binding by the malaria parasite. *Nat Commun.* 2016; 7:12837. [PubMed: 27667267]
14. Lau CK, et al. Structural conservation despite huge sequence diversity allows EPCR binding by the PfEMP1 family implicated in severe childhood malaria. *Cell Host Microbe.* 2015; 17:118–29. [PubMed: 25482433]
15. Lennartz F, Smith C, Craig AG, Higgins MK. Structural insights into diverse modes of ICAM-1 binding by *Plasmodium falciparum*-infected erythrocytes. *Proc Natl Acad Sci U S A.* 2019; 116:20124–20134. [PubMed: 31527263]
16. Colonna M, et al. A common inhibitory receptor for major histocompatibility complex class I molecules on human lymphoid and myelomonocytic cells. *J Exp Med.* 1997; 186:1809–18. [PubMed: 9382880]
17. Grakoui A, et al. The immunological synapse: a molecular machine controlling T cell activation. *Science.* 1999; 285:221–7. [PubMed: 10398592]
18. Dustin ML, Baldari CT. The Immune Synapse: Past, Present, and Future. *Methods Mol Biol.* 2017; 1584:1–5. [PubMed: 28255692]
19. Arora G, et al. NK cells inhibit *Plasmodium falciparum* growth in red blood cells via antibody-dependent cellular cytotoxicity. *Elife.* 2018; 7

20. Burrack KS, Hart GT, Hamilton SE. Contributions of natural killer cells to the immune response against Plasmodium. *Malar J.* 2019; 18:321. [PubMed: 31533835]
21. Winter G, et al. DIALS: implementation and evaluation of a new integration package. *Acta Crystallogr D Struct Biol.* 2018; 74:85–97. [PubMed: 29533234]
22. Winn MD, et al. Overview of the CCP4 suite and current developments. *Acta Crystallogr D Biol Crystallogr.* 2011; 67:235–42. [PubMed: 21460441]
23. McCoy AJ, et al. Phaser crystallographic software. *J Appl Crystallogr.* 2007; 40:658–674. [PubMed: 19461840]
24. Emsley P, Lohkamp B, Scott WG, Cowtan K. Features and development of Coot. *Acta Crystallogr D Biol Crystallogr.* 2010; 66:486–501. [PubMed: 20383002]
25. Bricogne GBE, Brandl M, Flensburg C, Keller P, Paciorek W, Roversi PSA, Smart OS, Vornhein C, Womack TO. BUSTER version 2.10.3. Cambridge, United Kingdom, Global Phasing Ltd. 2019
26. Bohme U, Otto TD, Sanders M, Newbold CI, Berriman M. Progression of the canonical reference malaria parasite genome from 2002-2019. *Wellcome Open Res.* 2019; 4:58. [PubMed: 31080894]
27. Edgar RC. MUSCLE: multiple sequence alignment with high accuracy and high throughput. *Nucleic Acids Res.* 2004; 32:1792–7. [PubMed: 15034147]
28. Crooks GE, Hon G, Chandonia JM, Brenner SE. WebLogo: a sequence logo generator. *Genome Res.* 2004; 14:1188–90. [PubMed: 15173120]
29. Shiroishi M, et al. Efficient leukocyte Ig-like receptor signaling and crystal structure of disulfide-linked HLA-G dimer. *J Biol Chem.* 2006; 281:10439–47. [PubMed: 16455647]
30. Iwanaga S, Kato T, Kaneko I, Yuda M. Centromere plasmid: a new genetic tool for the study of Plasmodium falciparum. *PLoS One.* 2012; 7:e33326. [PubMed: 22479383]
31. Hirayasu K, et al. Microbially cleaved immunoglobulins are sensed by the innate immune receptor LILRA2. *Nat Microbiol.* 2016; 1:16054. [PubMed: 27572839]
32. Choudhuri K, et al. Polarized release of T-cell-receptor-enriched microvesicles at the immunological synapse. *Nature.* 2014; 507:118–23. [PubMed: 24487619]
33. Alanine DGW, et al. Human Antibodies that Slow Erythrocyte Invasion Potentiate Malaria-Neutralizing Antibodies. *Cell.* 2019; 178:216–228. [PubMed: 31204103]

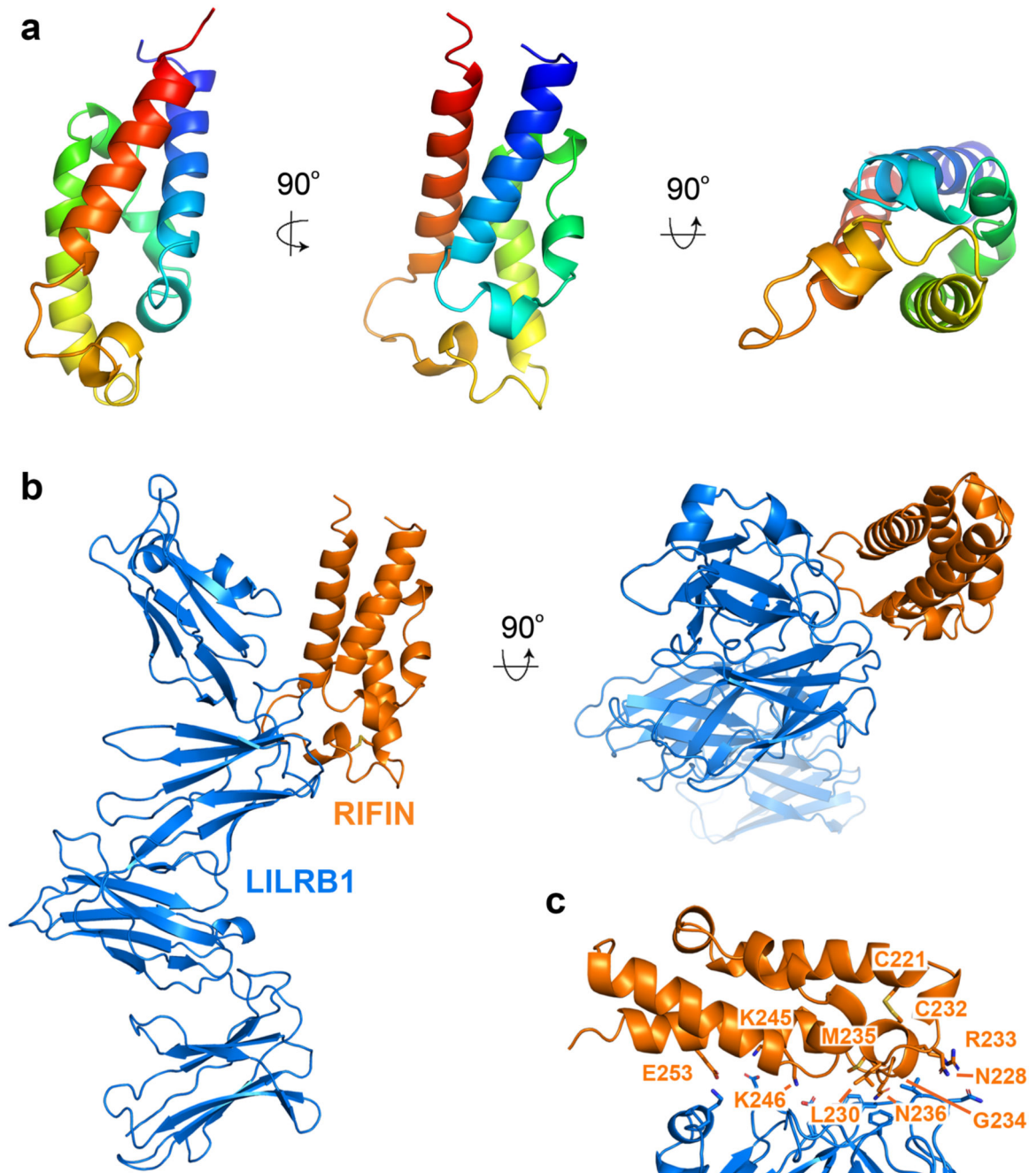


Figure 1. The structure of the RIFIN:LILRB1 complex.

a. The structure of RIFIN 1254800 variable region in a rainbow representation with N-terminus blue and C-terminus red. **b.** The structure of the RIFIN variable region (orange) bound to the LILRB1 ectodomain (blue). **c.** The interface between the RIFIN and LILRB1 with interacting residues and disulphide bonding cysteines of the RIFIN labelled in orange.

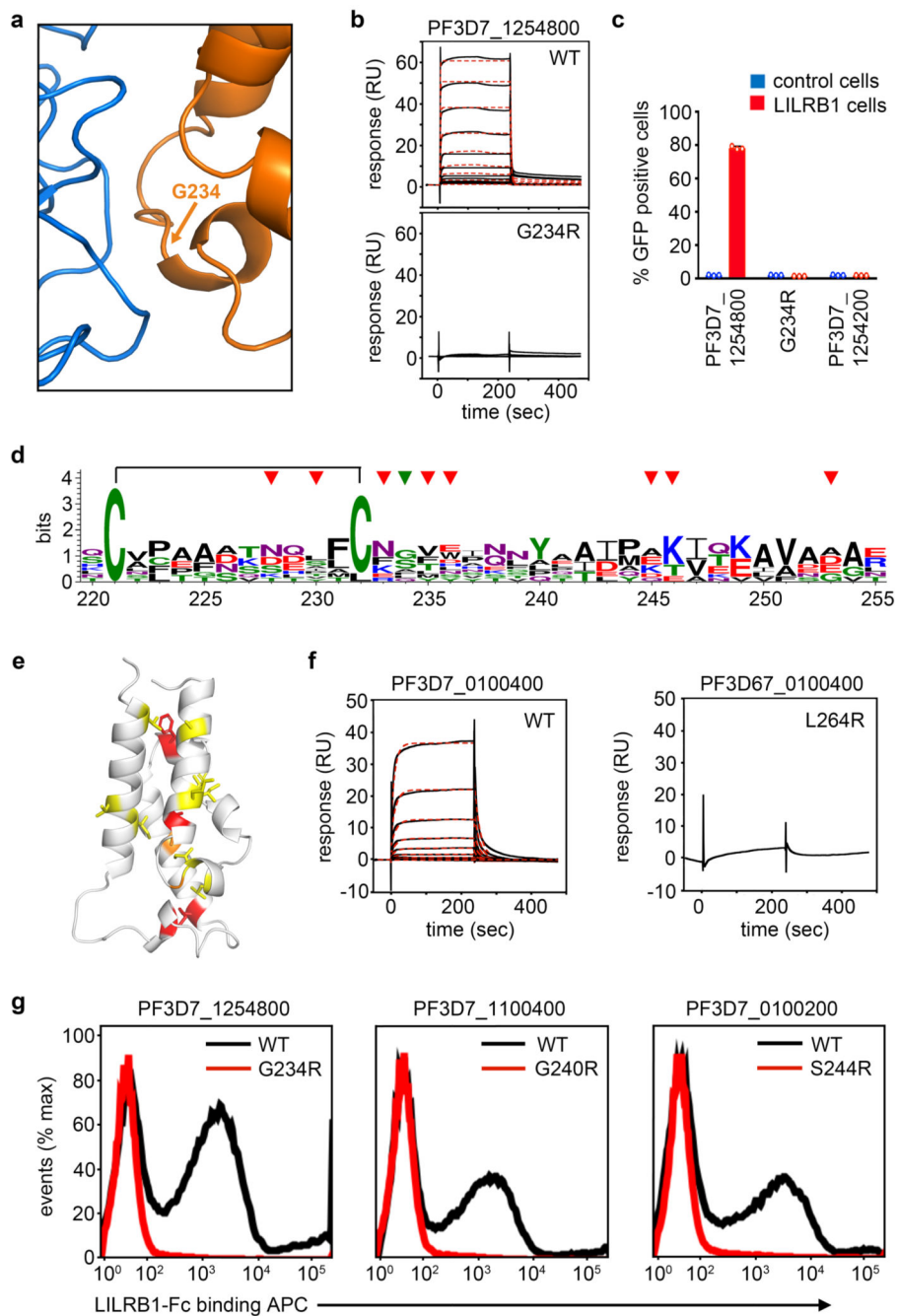


Figure 2. A conserved binding mode amongst sequence diverse LILRB1-binding RIFINs
a. A close up of the interface between the RIFIN and LILRB1 with residue G234 labelled. **b.** Surface plasmon resonance analysis of the binding of the RIFIN variable domain (WT: C223S) and its G234R (C223S G234R) mutant to immobilised LILRB1, injecting a two-fold dilution series from 4 μ M to 3.9nM. For the variable domain, equilibrium fitting gave $K_D = 700 \pm 5$ nM. Red dotted lines show the fitting to a one-to-one kinetic binding model and gave $K_D=1.04\mu$ M, $k_a=2.88 \times 10^5 M^{-1}s^{-1}$ and $k_d=0.299 s^{-1}$ ($\chi^2=3.76RU^2$) with $n=1$ for each series. **c.** Analysis of the effect of RIFIN (PF3D7_1254800), G234R and a non-LILRB1

binding RIFIN (PF3D7_1254200) on signalling in a T cell-based GFP reporter assay system. The mean of three independent measurements are shown with error bars representing the standard deviation. **d.** A sequence logo for residues from 10 LILRB1-binding RIFINs corresponding to residues 220-255 of PF3D7_1254800. Residues that contact LILRB1 are indicated with red triangles, G234 with a green triangle, and the conserved disulphide bond with a bracket. **e.** The most conserved residues in ten LILRB1-binding RIFINs plotted onto the structure of the RIFIN. Red represents a sequence entropy of <0.5 ; orange is 0.5-0.75 and yellow is 0.75-1.0. **f.** Surface plasmon resonance analysis for the binding of the variable domain of PF3D7_0100400 (injecting a two-fold dilution series from 8 μ M to 7.8nM) and its L264R mutant (8 μ M injection) to immobilised LILRB1. For the PF3D7_0100400, equilibrium fitting gave $K_D = 4.4 \pm 3.2 \mu\text{M}$. Red dotted lines show the fitting to a one-to-one kinetic binding model and gave $K_D=14.5\mu\text{M}$, $k_a=4100\text{M}^{-1}\text{s}^{-1}$ and $k_d=0.0592\text{s}^{-1}$ ($\chi^2=0.459\text{RU}^2$) with $n=1$ for each series. **g.** Flow cytometry analysis of the binding of LILRB1-Fc to erythrocytes infected with transgenic parasites expressing specific RIFINs and their mutants.

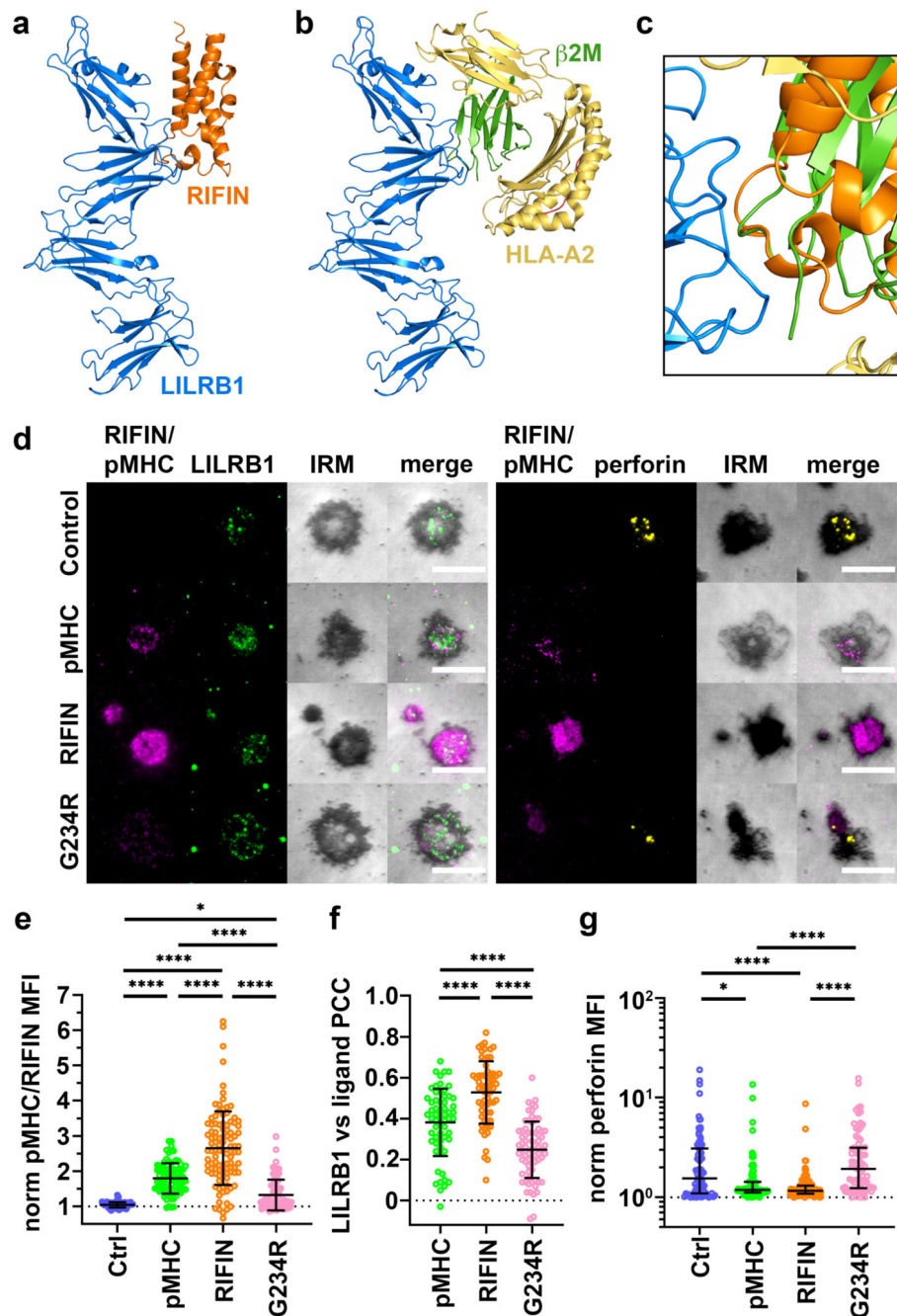


Figure 3. Molecular mimicry of MHC class I by a LILRB1-binding RIFIN reduces NK cell activation

a. Structure of the RIFIN variable region (orange) bound to LILRB1 (blue). **b.** A model of LILRB1 (blue) bound to MHC class I (alpha chain, yellow; b2-microglobulin, green), based on MHC class I bound to LILRB1 domains 1 and 2¹⁰. **c.** Close up of an alignment of RIFIN:LILRB1 complex with MHC class I:LILRB1 complex. **d.** Analysis of localisation of LILRB1 (green) or perforin (yellow) in the contact area for NK cells on SLBs coated with

RIFIN (C223S), G234R mutant (C223S G234R) or MHC class I (pMHC) (magenta). Scale bars = 10 μ m.

Measurements from three independent donors were pooled and analysed to investigate; **e.** the quantity of RIFIN (n=104 cells), G234R (n=78 cells) and pMHC (n=84 cells), with control (n=80 cells), in the contact area. All had adjusted p value < 0.0001 except for control versus G234R (p = 0.03); **f.** the degree of co-localisation of RIFIN (n=65 cells), G234R (n=71 cells) and pMHC (n=61 cells) with LILRB1. All had adjusted p value < 0.0001; and **g.** the quantity of perforin in the contact area. Control (n = 80 cells), pMHC (n = 84 cells), RIFIN (n = 104 cells), G234R (n = 78 cells). All had adjusted p value < 0.0001 except for control versus pMHC (p = 0.04), while control versus G234R and pMHC versus RIFIN were non-significant (p > 0.9999). Each data point represents the measurement from one cell. For e and f, Tukey's post hoc test was performed, and mean \pm 1 SD are shown. For g, Dunn's test was performed and median value \pm interquartile range is shown. *p < 0.05, **p < 0.01, ***p < 0.001, ****p < 0.0001. MFI = mean fluorescence intensity.